EARTHQUAKE SPECTRA

The Professional Journal of the Earthquake Engineering Research Institute

PREPRINT

This preprint is a PDF of a manuscript that has been accepted for publication in *Earthquake Spectra*. It is the final version that was uploaded and approved by the author(s). While the paper has been through the usual rigorous peer review process for the Journal, it has not been copyedited, nor have the figures and tables been modified for final publication. Please also note that the paper may refer to online Appendices that are not yet available.

We have posted this preliminary version of the manuscript online in the interest of making the scientific findings available for distribution and citation as quickly as possible following acceptance. However, readers should be aware that the final, published version will look different from this version and may also have some differences in content.

The DOI for this manuscript and the correct format for citing the paper are given at the top of the online (html) abstract.

Once the final, published version of this paper is posted online, it will replace the preliminary version at the specified DOI.

Fragility Curves for Wide-Flange Steel Columns and Implications on Building-Specific Earthquake-Induced Loss Assessment

Ahmed Elkady,[a] Subash Ghimire,[b] and Dimitrios G. Lignos,[c] M.EERI

Building-specific loss assessment methodologies utilize component fragility curves to compute the expected losses in the aftermath of earthquakes. Such curves are not available for steel columns assuming they remain elastic due to capacity design considerations. Nonetheless, first-story steel columns in moment-resisting frames (MRFs) are expected to experience damage, through flexural yielding and formation of geometric instabilities. This paper utilizes an experimental database that was recently assembled to develop two sets of univariate drift-based column fragility curves that consider the influence of loading history. Ordinal logistic regression is also employed to develop multivariate fragility curves that capture geometric and loading parameters that affect the column performance. The implications of the proposed fragility curves on building-specific loss assessment is demonstrated using a case of an 8-story office building with steel MRFs. It is shown that structural repair costs in this case may increase by 10%, regardless of the seismic intensity, when column damage is considered. Similarly, the contribution of structural component repairs to expected annual losses may double over the building lifespan.

INTRODUCTION

Within the performance-based earthquake engineering (PBEE) framework (Cornell and Krawinkler 2000; FEMA 2012), structural and non-structural damage control is a main objective in order to minimize the associated earthquake-induced economic losses in new and existing buildings (Aslani and Miranda 2005; FEMA 2012). Damage fragility curves are key components of this probabilistic framework. These curves relate the likelihood/probability of a component reaching or exceeding a specific damage state to a single predictor (i.e.,

[a] École Polytechnique Fédérale de Lausanne (EPFL), Lausanne, Switzerland
[b] University of Grenoble, Grenoble, France
[c] École Polytechnique Fédérale de Lausanne (EPFL), Lausanne, Switzerland

univariate fragilities) or multiple predictors (i.e., multivariate fragilities). Damage states are linked to pre-defined repair measures, allowing for the associated repair cost and time of repair to be quantified.

Univariate lognormal/normal cumulative distribution functions (CDFs) are the most prevalent form of fragility curves used in research and practice due to their simplicity. The predictor in this case is typically a story-based engineering demand parameter such as the story-drift ratio, *SDR* (i.e., drift-based fragility curves) or the peak floor absolute acceleration (i.e., acceleration-based fragility curves). A local engineering demand parameter, such as member rotation, is often used as well. Univariate fragility curves can be found in the literature for several key structural components, such as dissipative links in steel eccentrically-braced frames (Gulec et al. 2011), braces in steel concentrically-braced frames (Roeder et al. 2012; Lignos and Karamanci 2013), steel beam-to-column connections (Lignos et al. 2010; Ramirez et al. 2012), and reinforced concrete columns (Gardoni et al. 2002) as well as non-structural components (Taghavi and Miranda 2003; Ruiz-García and Negrete 2009; Retamales et al. 2013). A comprehensive database of univariate fragilities can be found in FEMA P-58 (FEMA 2012) for an extensive list of components of all construction materials.

Although univariate fragility curves are widely used, their limiting feature is that they cannot trace dependencies of damageable components to critical geometric, material, and loading parameters at a given *SDR*. To that end, bivariate and multivariate fragility curves are employed. For instance, Lignos and Karamanci (2013) proposed bivariate fragility curves to capture the dependency of inelastic steel brace buckling, to local and member slenderness. In a similar manner, Chiozzi and Miranda (2017) related cracking and crushing of masonry infill walls with masonry and mortar compressive strengths in addition to the *SDR*. Reed et al. (2016) developed fragility curves for electric power lifeline systems subjected to multiple weather hazards. Yazdi et al. (2016) demonstrated the applicability of multinomial ordinal logistic regression to produce multivariate fragility curves for reinforced concrete shear walls. This type of regression is commonly used within the social and medical science disciplines.

Capacity-designed steel moment-resisting frames (MRFs) dissipate the seismic energy through flexural yielding of the beams and controlled/limited shear yielding of the panel zones. Steel MRF columns are supposed to remain elastic except at the first-story column

base. Research indicates that column yielding and/or buckling may occur in other locations along the height of a steel MRF building subjected to low-probability of occurrence earthquakes (Gupta and Krawinkler 2000; Elkady and Lignos 2014, 2015b). This may very well be the case in existing steel MRF buildings designed with pre-Northridge connections (Lee and Foutch 2002) or constructed prior to the Uniform Building Code (UBC 1973) provisions (i.e., without capacity design considerations) (Hutt et al. 2016).

Currently, there are no fragility curves available for steel wide-flange columns. This is due to (1) the limited amount of experimental data on seismically compact steel wide-flange columns till recently; and (2) the assumption that steel columns in capacity-designed buildings, remain elastic during earthquakes (FEMA 2012). In that respect, steel beam fragility curves are typically utilized to quantify the extent of column damage for building-specific loss assessment of steel MRFs (Hwang and Lignos 2017). Experimental research on the seismic behavior of wide-flange steel columns (Popov et al. 1975; MacRae et al. 1990; Newell and Uang 2006; Suzuki and Lignos 2015; Elkady and Lignos 2016; Lignos et al. 2016; Ozkula et al. 2017) suggests that steel column limit states are fairly different than those observed in steel beams. In particular, the extent of column damage is strongly dependent on the applied axial load demand, and the local and member slenderness in addition to the magnitude of lateral drift demands. As such, the development of steel column fragility curves is necessary.

This paper discusses the development of damage fragility curves for seismically compact wide-flange steel MRF columns. This is achieved through an assembled experimental database of steel columns subjected to multi-axis cyclic loading. Both univariate drift-based and multivariate fragilities are developed. The former can be used in rapid damage assessment while the latter facilitates a more accurate damage estimate once additional column parameters are known. In addition, two sets of univariate fragilities are developed to assess differences due to the imposed employed loading history seen in design basis and low-probability earthquakes. Each set can be utilized depending on the target performance level and seismic intensity. Finally, the influence of the proposed fragility curves is quantified through building-specific loss assessment at selected seismic intensities of interest to the engineering profession.

DESCRIPTION OF STEEL COLUMN EXPERIMENTAL DATABASE

The steel column database comprises of 38 column specimens collected from five different testing programs (MacRae et al. 1990; Suzuki and Lignos 2015; Lignos et al. 2016; Ozkula et al. 2017; Elkady and Lignos 2018a). The geometric data of the collected specimens are summarized in Table 1. In this table, h/t_w and $b_f/2t_f$ are the web and flange slenderness ratios, respectively, and L_b/r_y is the column's member slenderness ratio. Table 1 also summarizes the applied axial load ratio, P_c/P_{yn}, in which, P_c is the applied constant compressive load and P_{yn} is the column's axial yield strength based on the measured geometric properties of the respective column's cross-section and the nominal yield stress of the steel material.

Figure 1 illustrates the distribution of the geometric parameters as well as the axial load ratio of the collected data. In brief, the database covers columns within the following ranges: $17 \leq h/t_w \leq 52.7$, $4.8 \leq b_f/2t_f \leq 9.2$, $13 \leq L_b/r_y \leq 160$, and $0.0 \leq P_c/P_{yn} \leq 0.87$. This includes hot-rolled wide-flange columns with sizes ranging from shallow W10 and W14 to deep W24 cross-sections. Figure 1 shows that 24 specimens utilize cross-sections that satisfy the local slenderness limits for highly ductile members, λ_{hd} according to ANSI/AISC 341-16 (AISC 2016a). The remaining specimens satisfy the moderately ductile limits, λ_{md}, of the same provisions. Only specimens that were systematically subjected to a unidirectional symmetric cyclic lateral loading history combined with constant compressive axial load were considered. This was done intentionally to reduce the scatter due to the dependency of the column response on the imposed lateral loading history (Krawinkler 1996; Suzuki and Lignos 2015; Elkady and Lignos 2018a). As such, the proposed steel column fragility curves are consistent with the ones presented in FEMA P58 (FEMA 2012). However, the influence of the loading history on the steel column fragilities is discussed in detail later in the paper.

DEFINITION OF STEEL COLUMN DAMAGE STATES

Figures 2a and 2b show the typical moment-rotation and axial shortening-rotation relations, respectively, of a column subjected to a symmetric lateral loading history coupled with constant compressive axial load. The x-axis in these two figures represents the column chord-rotation calculated as $SDR_C = \delta_c / L$ as illustrated in Figure 2c, where δ_c is the lateral drift at the column's top end due to flexure and shear in the column and L is the column's undeformed length. Note that SDR_C excludes story drifts, δ_b and δ_p, due to beam rotation (θ_b) and panel-zone distortion (θ_p), respectively. Table 2 summarizes five sequential damage states, labeled DS_1 to DS_5. These limit states reflect different magnitudes of steel column

flexural strength deterioration and axial shortening. The five limit states, which are based on observations from wide-flange steel column experiments, are described below in detail.

Table 1. Steel column experimental database – symmetric loading history and constant compressive axial load

Reference	#	Section	Geometric properties*			$\frac{P_c}{P_{yn}}$	SDR_C [% rad]				
			$\frac{h}{t_w}$	$\frac{b_f}{2t_f}$	$\frac{L_b}{r_y}$		DS_1	DS_2	DS_3	DS_4	DS_5
MacRae et al. (1990)	1	W10x49	25.9	9.2	13	0.01	0.51	4.10	-	-	-
	2	W10x49	25.9	9.2	13	0.36	0.44	2.00	3.80	-	-
	3	W10x49	25.9	9.2	13	0.45	0.36	1.00	3.50	4.00	3.90
	4	W10x49	25.9	9.2	13	0.57	0.26	1.00	2.30	-	-
	5	W10x49	25.9	9.2	13	0.71	0.24	0.80	3.00	-	-
	6	W10x49	25.9	9.2	13	0.79	0.18	0.60	2.00	-	-
	7	W10x49	25.9	9.2	13	0.87	0.15	0.55	1.50	-	-
Suzuki and Lignos (2015)	8	W14x53	28.6	6.3	38	0.33	0.64	1.75	3.50	4.50	5.20
	9	W14x61	29.7	8.1	30	0.33	0.74	1.60	3.50	-	-
	10	W14x82	17.0	6.0	30	0.33	0.73	3.20	4.00	5.20	6.40
Ozkula et al. (2017)	11	W24x176	27.5	4.8	71	0.18	0.82	4.00	6.30	-	-
	12	W24x176	27.5	4.8	71	0.36	0.67	2.00	3.30	4.00	-
	13	W24x176	27.5	4.8	71	0.54	0.49	1.50	2.00	-	-
	14	W24x131	34.2	6.7	72	0.00	0.84	4.80	-	-	-
	15	W24x131	34.2	6.7	72	0.18	0.77	3.00	4.00	-	-
	16	W24x131	34.2	6.7	72	0.36	0.62	1.50	2.30	2.90	-
	17	W24x131	34.2	6.7	72	0.36	0.62	1.50	2.30	2.90	3.80
	18	W24x131	34.2	6.7	72	0.54	0.42	0.75	1.10	-	-
	19	W24x131	34.2	6.7	72	0.54	0.45	0.75	1.10	1.50	-
	20	W24x131	34.2	6.7	72	0.36	0.64	1.50	2.00	-	-
	21	W24x104	41.7	8.5	73	0.18	0.73	1.50	3.25	4.00	-
	22	W24x104	41.7	8.5	73	0.36	0.65	0.75	1.50	-	-
	23	W24x104	41.7	8.5	73	0.54	0.44	0.75	0.80	-	-
	24	W24x84	44.2	5.8	110	0.18	0.73	1.50	3.00	-	-
	25	W24x84	44.2	5.8	110	0.18	0.70	2.00	3.00	-	-
	26	W24x84	44.2	5.8	110	0.36	0.61	1.00	1.50	-	-
	27	W24x55	52.7	7.0	160	0.18	0.70	1.00	1.50	-	-
	28	W24x55	52.7	7.0	160	0.27	0.65	0.88	1.00	-	-
	29	W24x55	52.7	7.0	160	0.36	0.54	0.75	0.75	-	-
Elkady and Lignos (2018a)	30	W24x146	30.5	6.1	52	0.24	0.57	1.50	3.00	4.00	5.30
	31	W24x146	30.4	6.1	52	0.60	0.32	0.72	1.50	2.00	2.00
	32	W24x146	30.7	6.1	52	0.24	0.70	2.00	3.00	4.40	5.90
	33	W24x146	29.6	5.9	52	0.23	0.62	2.00	3.00	4.00	5.10
	34	W24x84	43.0	6.1	79	0.19	0.59	1.50	3.00	4.00	4.50
	35	W24x84	43.7	6.1	79	0.19	0.54	1.40	3.00	4.00	4.50
Lignos et al. (2016)	36	W14x82	20.6	5.9	29	0.57	0.47	1.95	3.00	4.00	-
	37	W14x82	22.1	5.9	28	0.84	0.23	1.00	2.00	3.00	3.20

38	W16x89	26.5	6.0	29	0.52	0.39	0.80	2.50	3.10	-

*h: web height; t_w: web thickness; b_f: flange width; t_f: flange thickness; L_b: laterally unsupported length; r_y: radius of gyration in the weak-axis orientation

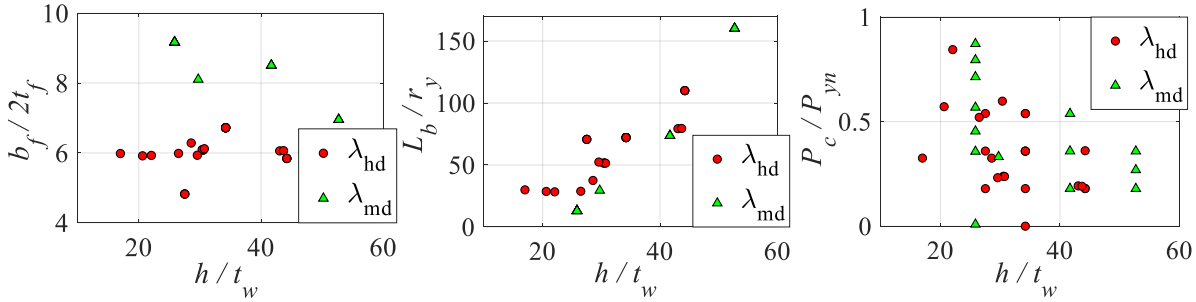

Figure 1. Distribution of local slenderness ratios, member slenderness and axial load ratios for the collected steel column database

Table 2. Summary of damage states

ID	Description	Notation	No. of data points (N)
DS_1	Onset of yielding	Y	38
DS_2	Onset of local buckling	LB	38
DS_3	20% loss in maximum flexural strength 50mm axial shortening	MD (Moderate Damage)	36
DS_4	50% loss in maximum flexural strength 100mm axial shortening	SD (Severe Damage)	16
DS_5	80% loss in maximum flexural strength 120mm axial shortening	ED (Excessive Damage)	11

DS_1: Onset of Yielding

This damage state is related to the first occurrence of flange and/or web yielding near the column ends as shown in Figure 2d. Because there is no reduction in the column's strength and/or stiffness associated with column yielding, repair actions are mainly cosmetic. In particular, repainting of the pealed steel surface, repairs for cracked/displaced architectural enclosures and finishes in the vicinity of the column ends should suffice.

A consistent definition of the $SDR_{C,Y}$ is adopted to circumvent the ambiguity related to reported $SDR_{C,\,Y}$ values at yielding from each experimentalist. In particular, $SDR_{C,\,Y}$ is deduced analytically based on the extreme cross-section fiber reaching the measured yield stress. Equation (1) is employed for this purpose,

$$SDR_{C,\,Y} = M_y^* / K_e \tag{1}$$

In which, M_y^* is the reduced flexural yield capacity calculated based on ANSI/AISC 360-16 (AISC 2016b) axial load-bending interaction (i.e., P-M) equations, where the measured

material and geometric properties are utilized, and K_e is the column's effective flexural stiffness considering both flexural and shear deformations. Note that K_e correlates well with the measured stiffness from the moment-rotation relation (see Figure 2a). In particular, the difference between the two did not exceed 10% across the different testing programs.

DS_2: Onset of Local Buckling

The second damage state is associated with the onset of web and/or flange local buckling as shown in Fig. 2e. In seismically compact columns, the onset of local geometric instabilities is associated with flexural strength deterioration. Accordingly, this damage state is deduced here as the SDR_C at which the maximum flexural strength, M_{max}, is reached (i.e., $SDR_{C,\,LB}$) as illustrated in Figure 2a. Repair efforts in this case involve shoring of the column followed by heat straightening of the buckled web and flanges (FEMA 2012).

DS_3, DS_4, and DS_5: Different Levels of Column Axial Shortening and Corresponding Loss of Flexural Strength

Figure 3 shows that there is a strong correlation between SDR_C values corresponding to discrete amplitudes of local buckling-induced shortening and those corresponding to discrete levels of flexural strength deterioration (see Figures 2a and 2b). In these plots, Δ_{axial} was consistently deduced to represent the amount of axial shortening resulting from local buckling at one column end. In Figure 3c, only four data points are plotted because axial shortening was measured and reported only in 4 out of 8 specimens that reached 20% M_{max}. However, these correlations were further verified based on parametric finite element simulations conducted recently by the authors (Elkady and Lignos 2017).

Based on these observations, DS_3, DS_4 and DS_5 are defined. Each one represents a specific percentage loss in maximum flexural strength, M_{max}, and a given amplitude of column axial shortening. In particular, in DS_3 a column cannot sustain more than 80% M_{max} and the corresponding axial shortening is 50mm (equivalent to 1.25% of a typical 4m (13ft) long column). Similarly, in DS_4 a column cannot sustain more than 50% M_{max} and the corresponding axial shortening is 100mm (2.5% L); in DS_5 a column cannot sustain more than 20% M_{max} and the corresponding axial shortening is 120mm (3% L). In order to couple column axial shortening with an associated flexural strength loss, within the same damage state, the corresponding SDR_C is taken as the larger of the two SDR_C values based on the strength loss and column shortening limit states. In summary, DS_3, DS_4 and DS_5 represent

Moderate (MD), Severe (SD), and Excessive (ED) column damage, as indicated by Figs. 2e to 2g, respectively.

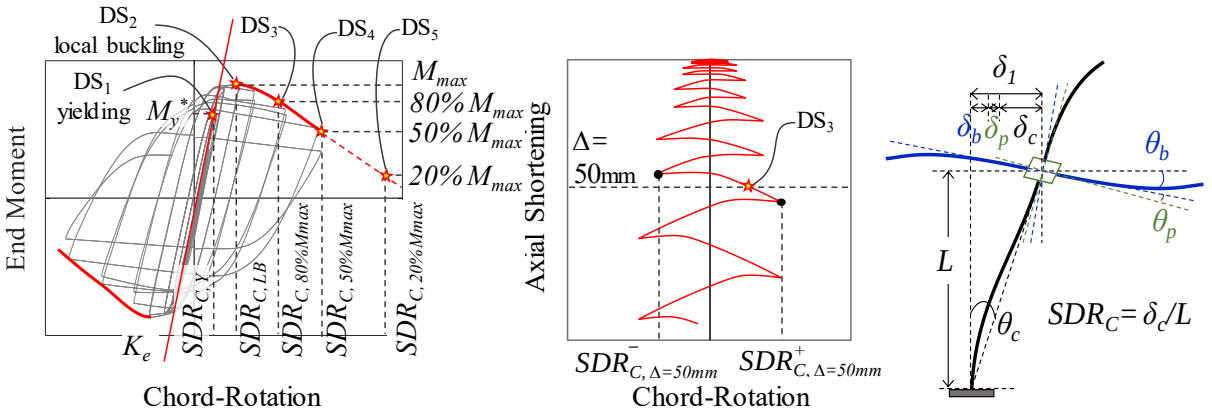

(a) typical hysteretic response under sym. cyclic loading and constant axial load

(b) typical axial shortening history under sym. cyclic loading

(c) definition of column rotation

(d) DS_1: onset of yielding (Y)

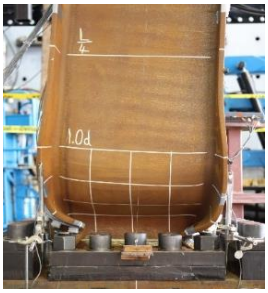

(e) DS_2: onset of local buckling (LB)

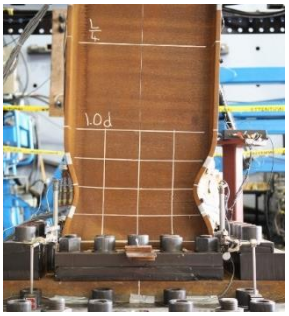

(f) DS_3: moderate damage (MD)

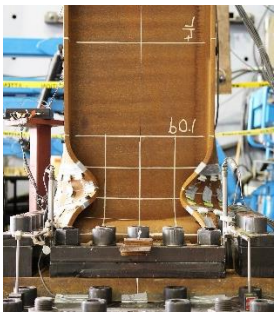

(g) DS_4: severe damage (SD)

(h) DS_5: excessive damage (ED)

Figure 2. Definition of damage states for wide-flange steel columns [photos from Suzuki and Lignos (2015) and Elkady and Lignos (2018a)

In brief, the SDR_C values at which these three damage states occur is deduced from the first-cycle envelope curve fitted to the moment-rotation hysteretic data, as illustrated in Figure 2a. The average of the positive and negative SDR_C amplitudes is employed to define the associated SDR_C value corresponding to the DS of interest. Note that DS_5 was only reached in eight specimens. In most cases, steel columns with stocky cross-sections subjected

to low axial load ratios are the ones that did not reach DS_5. In other cases, the steel column was not sufficiently pushed to large lateral drifts due to safety and/or laboratory limitations. Therefore, to complement the data for DS_5, the post-peak slope of the first-cycle envelope is extrapolated beyond DS_4 as illustrated in Figure 2a. Referring to Figure 2b, the average of the peak SDR_C values preceding and succeeding reaching a given amplitude of axial shortening is employed. Note that given how the damage states are deduced, it is possible for two or more damage states to have the same *SDRc* value (e.g., DS_4 and DS_5 of specimen #31).

For DS_3, the repair effort is similar to that of DS_2 because the extent of local buckling is still repairable. In DS_4 and DS_5, the column is severely damaged (see Figures 2g and 2h) and global instabilities associated with twisting are likely to occur as shown in Figure 2h (Elkady and Lignos 2018a). Hence, repair through heat straightening will be neither effective nor feasible. Shoring and replacing the entire column might be the only repair option in this case (FEMA 2008). However, this repair type is rarely performed considering that DS_4 and DS_5 imply large residual deformations under which the building may have to be demolished as a whole. Although for all practical reasons, DS_4 and DS_5 are similar; the latter is included to complement the ordinal logistic regression analysis discussed later in the paper.

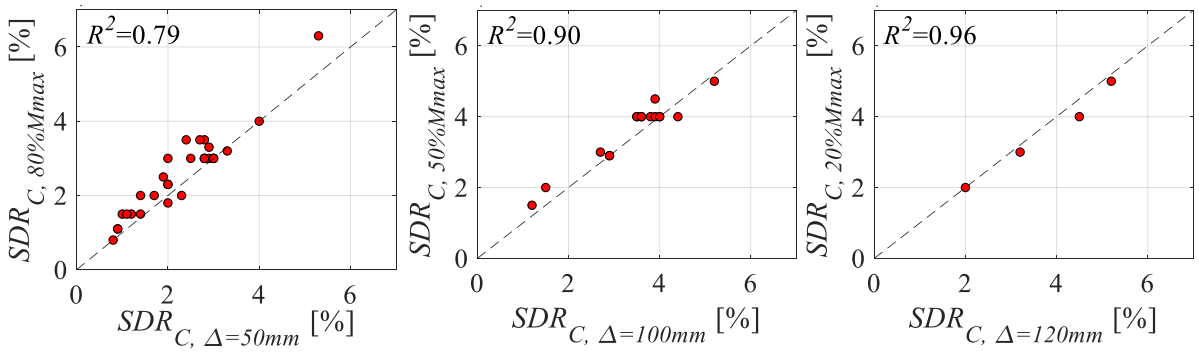

(a) DS_3 (b) DS_4 (c) DS_5

Figure 3. Correlation between axial shortening and flexural strength for selected damage states

UNIVARIATE DRIFT-BASED FRAGILITY CURVES

Figure 4a shows the SDR_C distributions for each one of the five damage states discussed in the previous section. The median SDR_C values are superimposed in dashed lines. These individual SDR_C values for each specimen are also summarized in Table 1. Using the observed SDR_C values, an empirical cumulative distribution function (CDF) is fitted for each damage state. This is done by sorting the absolute SDR_C values in ascending order and then calculating the cumulative probability, p_i, as i/n; where, n is the total number of data points

(see Table 2) and *i* is the order of a given data point after sorting. Figure 4b shows the empirical CDF, in round markers, of DS_2 as an example.

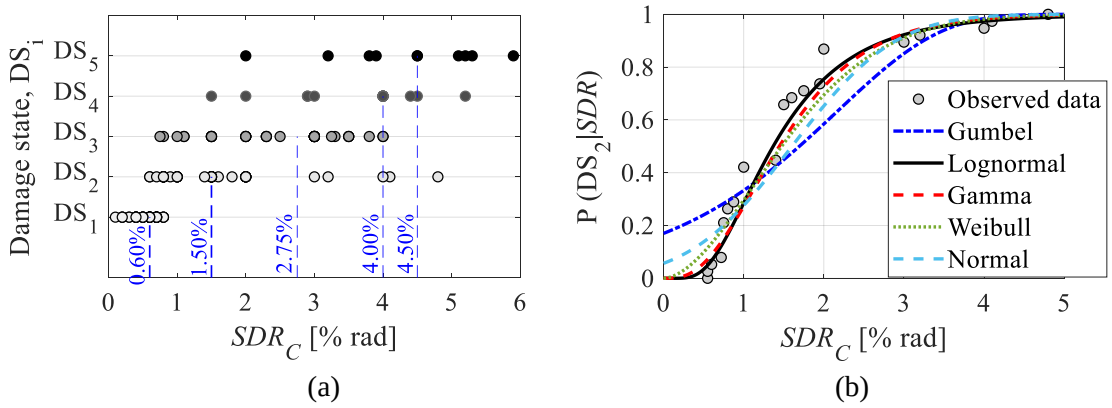

Figure 4. (a) Distribution of SDR_C values for each damage state; (b) illustration of fitted distributions for DS_2

Five probability distribution functions (i.e., Gamma, Gumbel, Weibull, Normal and Lognormal) were fitted to the empirical CDFs. Figure 4b shows the fitted probability distributions for DS_2. The Kolmogorov-Smirnov (K-S) goodness-of-fit test (Kolmogorov 1933; Smirnov 1939) was performed to verify the suitability of each theoretical distribution for modeling the underlying population at the 5% significance level. Based on this test, the gamma and lognormal cumulative probability distributions adequately fit the empirical CDFs regardless of the damage state of interest. Therefore, the lognormal probability distribution is selected for consistency with other structural and non-structural fragility curves described in FEMA-P58 (FEMA 2012). The lognormal CDF is given by Equation 2, in which, $P(DS_i|SDR_C)$ is the conditional probability of reaching or exceeding damage state *i*, at a given SDR_C; Φ is the cumulative standard normal distribution; μ_{SDRC} is the central tendency of the dataset; and $\sigma_{\ln SDRC}$ is the standard deviation of the associated normal distribution.

$$P(DS_i \mid SDR_C) = \Phi\left(\frac{\ln(SDR_c) - \ln(\mu_{SDR_C})}{\sigma_{\ln SDR_C}}\right) \quad (2)$$

Figure 5 shows for reference the fitted lognormal distrbutions for three damage states DS_1, DS_2, and DS_4. The population parameters of the lognormal distribution (μ_{SDRC} and $\sigma_{\ln SDRC}$) are estimated based on the maximum likelihood approach and are summarized in Table 3.

It is worth noting that specimens subjected to constant compressive axial load demands, as those employed herein, are representative of interior MRF columns. End or exterior columns, however, can experience large variations in axial load demands due to dynamic overturning

effects. This results in an asymmetric cyclic response where damage is exacerbated in one loading direction (with increasing compressive loads) and relieved in the other direction (with decreasing compressive or increasing tensile loads). Given the limited number of tests on such columns, discussion herein is restricted to those under constant axial loads. Nonetheless, it is worth noting that significant difference in the level of damage in interior and exterior columns is to be expected at story drift-ratios larger than 2% (Suzuki and Lignos 2015; Lignos et al. 2016; Elkady et al. 2018). In that respect, fragility curves for DS_1 to DS_3 may be used in both cases. For end columns the gravity-induced load ratio may be used as suggested by Hartloper and Lignos (2017).

Similarly, the employed specimens herein were subjected to unidirectional lateral loading. Under an actual earthquake, MRF columns will undergo bidirectional drift demands. Experimental observations by Elkady and Lignos (2018a) showed that the column's lateral stiffness deteriorates more due to global instabilities triggered by bidirectional loading at story drift-ratios larger than 3% (succeeding DS_3), compared to unidirectional loading. Excluding this difference, the column response remains practically unaffected.

Table 3. Population parameters for univariate drift-based lognormal fragility curves for steel columns

Damage state	μ_{SDR_C}	$\sigma_{\ln SDR_C}$	$\mu_{SDR_C}\|90\%CI$ (lower, upper)	$\sigma_{\ln SDR_C}\|90\%CI$ (lower, upper)
DS_1 (Y)	0.507	0.425	0.490, 0.526	0.358, 0.526
DS_2 (LB)	1.368	0.552	1.306, 1.434	0.465, 0.684
DS_3 (MD)	2.292	0.491	2.197, 2.392	0.412, 0.613
DS_4 (SD)	3.502	0.321	3.359, 3.651	0.248, 0.461
DS_5 (ED)	4.336	0.327	4.120, 4.564	0.242, 0.521

Epistemic Uncertainty

Specimen-to-specimen variability is reflected in the standard deviation $\sigma_{\ln SDRC}$ of the developed fragility curves. The uncertainty associated with the finite data set is incorporated herein by computing asymmetric confidence intervals of the lognormal CDF's standard deviation and mean using Equation 3 and 4, respectively, as discussed in Crow et al. (1960). In Equation 3, $\chi^2_{\alpha/2,n-1}$ and $\chi^2_{1-\alpha/2,n-1}$ are the inverse of the χ^2 (chi-square) distribution having n-1 degree of freedom and probability of occurrence of $\alpha/2$ and 1-$\alpha/2$, respectively.

$$\left(\frac{(n-1)}{\chi^2_{\alpha/2,n-1}}\right)^{1/2}\cdot\sigma_{\ln SDR_C} \text{ and } \left(\frac{(n-1)}{\chi^2_{1-\alpha/2,n-1}}\right)^{1/2}\cdot\sigma_{\ln SDR_C} \quad (3)$$

$$\mu_{SDR_C} \cdot \exp\left(\pm Z_{\alpha/2} \cdot \frac{\sigma_{\ln SDR_C}}{\sqrt{n}}\right) \quad (4)$$

In Equation 4, $Z_{\alpha/2}$ is the value of the standard normal distribution such that the probability of a random deviation numerically greater than $Z_{\alpha/2}$ is α. Table 3 summarizes the μ_{SDRc} and $\sigma_{\ln SDRc}$ values at the 10% and 90% confidence interval (CI) for each damage state, in line with FEMA (2012) guidelines. The uncertainty envelopes are superimposed for illustration in Figure 5. These envelopes are useful to compute the upper and lower bound probability of reaching or exceeding DS_i if SDR_C is used as single predictor. For instance, the 50% probability of exceeding DS_4 (SD) lies between SDR_C=3.3% and 3.8% rad (see Figure 5d). Similarly, the probability of reaching or exceeding DS_4 at SDR_C=3% varies from 20% to 40%. This simple example highlights the importance of incorporating epistemic uncertainties into the proposed univariate fragility curves for wide flange steel columns.

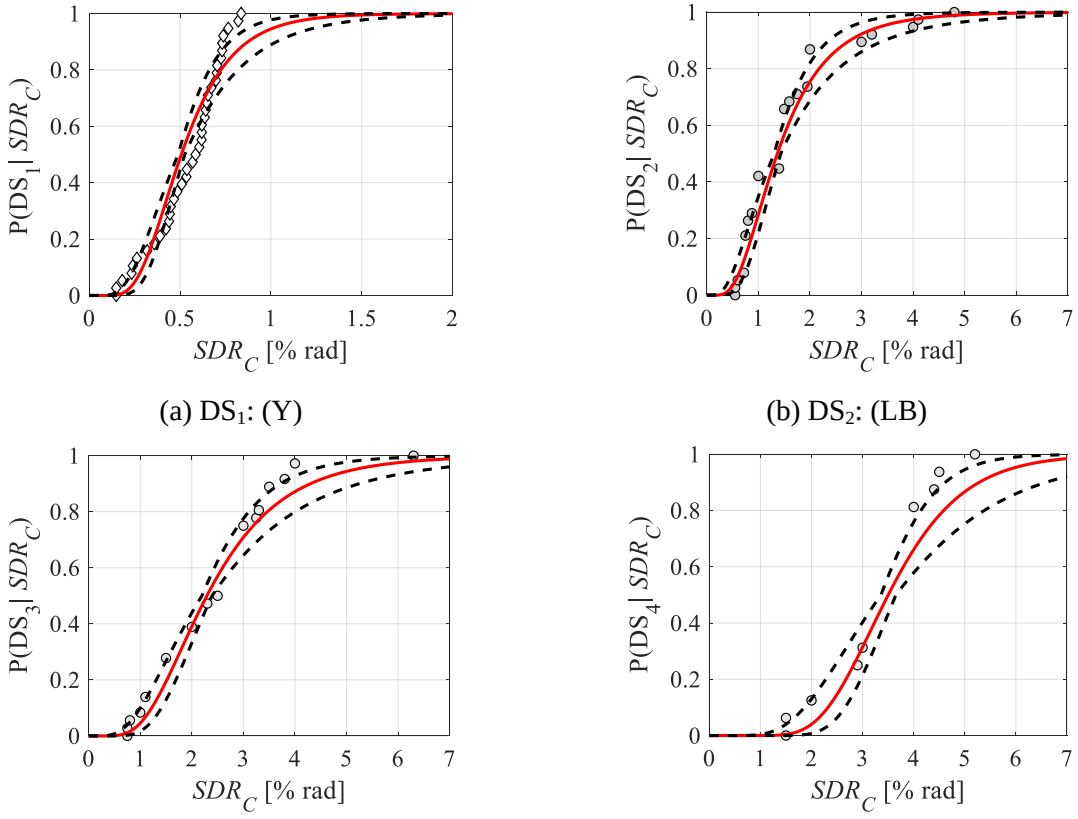

(a) DS_1: (Y) (b) DS_2: (LB)

(c) DS_3: (MD) (d) DS_4: (SD)

Figure 5. Fitted lognormal CDFs (*solid line*) along with uncertainty envelopes (*dashed lines*) at the 10% and 90% confidence level

MULTIVARIATE FRAGILITY CURVES

Experimental work highlighted the dependency of the steel column stability on the local and member slenderness, the imposed lateral loading history and the applied axial load demands (MacRae et al. 1990; Suzuki and Lignos 2015; Lignos et al. 2016; Ozkula et al. 2017; Elkady and Lignos 2018a). Multiple linear or nonlinear regression cannot be used herein to capture the aforementioned dependencies within a fragility curve because the dichotomous (i.e., binary) response variable (i.e., the probability of an event occurring/not-occurring) that should be modeled does not follow a normal distribution (a condition that needs to be satisfied for most regression types). Instead, ordinal logistic regression (OLR) (McCullagh 1980), is employed to develop multivariate fragility curves. Such regression type can be used when there are two, or more, dichotomous response variables that have a sequential order.

In logistic regression, the continuous probability function between the discrete binary probability values of 0 and 1 is captured using a link function. The most commonly used form is the *logit* function. This function has an "S" shape (i.e., sigmoid curve) in which the dependent variable boundaries (probability in this case) are positive real numbers between 0 and 1. The multinomial logistic regression model, used herein for the ordinal type of data, is expressed by Equation 5. The *logit* function (left-hand side of Equation 5) is expressed as a linear combination of the products of each predictor variable and its associated regression coefficients (right-hand side of Equation 5). In this equation, p_j is the probability of reaching damage state j or less [i.e., $P(DS \leq ds_j)$]; k is the number of damage states; m is the number of predictor variables; α_j is the intercept parameter; and the β_i parameters are the model coefficients for each predictor variable V_i. The left side of Equation 5 also represents the natural logarithm of the odds of reaching damage state j or less. Note that ordinal logistic regression assumes proportional odds ratio where a unit change in any independent variable V_i (while other variables remain constant) causes equal effect on the ordinal dependent variable(s) (i.e, odds), regardless of the location within the V_i range.

$$\ln\left(\frac{p_j}{1-p_j}\right) = \alpha_j + \beta_1 V_1 + \beta_2 V_2 + \beta_3 V_3 + ... + \beta_m V_m \ , \qquad j = 1, 2, 3, ...k-1 \tag{5}$$

Pilot studies by the authors (Elkady and Lignos 2015a, 2017, 2018b) suggest that h/t_w, L_b/r_y, and P_c/P_{yn} have a statistically significant effect on the column response parameters. This is demonstrated in Figure 6 for DS_3 vis-à-vis the above discussion. Therefore, the predictor variables of the regression model include the three aforementioned parameters, the

$b_f/2t_f$, and the natural logarithm of the SDR_C, expressed as a percentage. This model is referred to here as "Model 1" and is expressed as follows,

$$\ln\left(\frac{p_j}{1-p_j}\right) = \alpha_j + \beta_{h/tw}\frac{h}{t_w} + \beta_{bf/2tf}\frac{b_f}{2t_f} + \beta_{Lb/ry}\frac{L_b}{r_y} + \beta_{Pc/Pyn}\frac{P_c}{P_{yn}} + \beta_{\ln(SDR_C)}\ln(SDR_C) \quad (6)$$

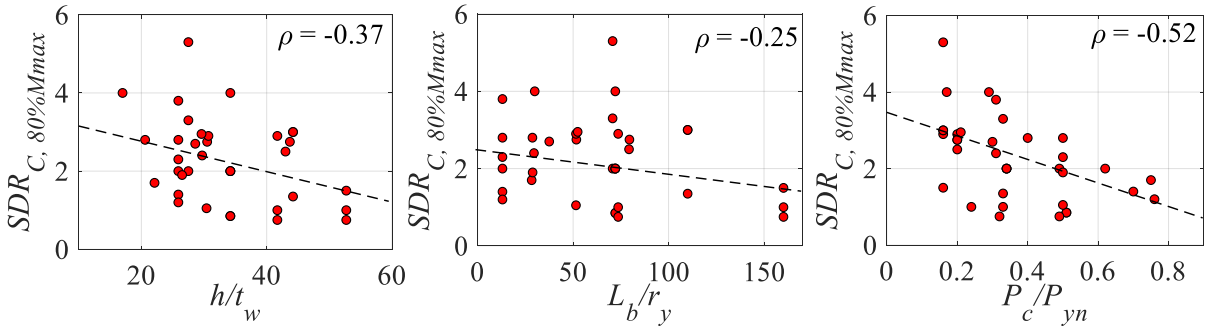

Figure 6. Correlation between DS_3 and selected predictor variables

To conduct multinomial OLR, observation data points are needed. These observation points must represent the SDR_C values between the different damage states, rather than the transition SDR_C values discussed earlier (see Figure 2a and Table 1). To that end, OLR can be conducted with a minimum of two observation points at each damage state (right before and right after the occurrence of a given damage state). However, if more observation points are included then the statistical uncertainty (i.e., a narrower confidence band) of the fragility curves can be reduced (Yazdi et al. 2016). Five observation SDR_C points are employed here between each two consecutive damage states as illustrated in Fig. 7. In particular, observation points 1 and 5 have a small finite offset of 0.005% rad from the transition SDR_C values of the preceding and succeeding damage states, respectively. Observation points 2, 3, and 4 are equally allocated between observation point 1 and 5. Table 4 summarizes the observation point values between DS_2, DS_3, and DS_4 for a sample specimen.

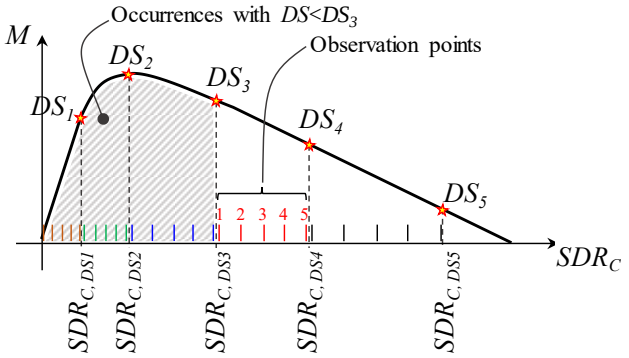

Figure 7. Illustration of observation points allocation between damage states

Table 4. Deduced observation points for a sample specimen

			SDR_C [% rad]											
#	Section	**DS_2**	Observation points					**DS_3**	Observation points					**DS_4**
			1	2	3	4	5		1	2	3	4	5	
35	W24x84	**1.40**	1.405	1.800	2.200	2.600	2.995	**3.00**	3.005	3.250	3.500	3.750	3.995	**4.00**

Ordinal logistic regression is conducted with SPSS (2017). Although five predictors are used in Model 1, some of them have greater influence on the associated column damage compared to others. As such, Model 1 can be simplified by removing the less influential predictors while maintaining the robustness of the regression model. The coefficient of variation (*COV*) of each regression coefficient, β, is first evaluated based on Model 1. The predictor associated with the largest *COV* is then eliminated and OLR is repeated with the remaining variables. This process was proposed by Gardoni et al. (2002) and used in Yazdi et al. (2016) for reinforced concrete shear walls. In parallel with this process, the overall regression model robustness should be evaluated following each predictor removal. The residual deviance (*RD*) is used for this purpose.

Table 5 summarizes the *COV* values for each predictor based on Model 1. The $b_f/2t_f$ term had the largest *COV* of 114.2%. This is attributed to the strong correlation between, $b_f/2t_f$ and h/t_w in hot rolled wide-flange cross-sections. Accordingly, this term was removed and the regression was performed for the new model (i.e., Model 2). Removing this predictor did not affect the model quality since the increase in the residual deviance was practically zero (≈0.02%). Similarly, in Model 2, L_b/r_y had a large *COV* of 43.0%. Removing this term increased the residual deviance by 0.6%, which again is deemed insignificant. The reason is that L_b/r_y is typically associated with member instabilities (i.e., lateral torsional buckling) that are not pronounced in DS_1 to DS_3 (Elkady and Lignos 2018a) for typical steel column ranges. The severity of multi-collinearity among the predictors, in the regression model, was checked using the variance inflation factor (*VIF*) (Kutner et al. 2004). This factor indicates how much larger the standard error is, compared with what it would be if a given predictor was uncorrelated with respect to the other model predictors. As a rule of thumb, the data have a multi-collinearity problem if *VIF* is greater than 10 (Chatterjee and Hadi 2015). The *VIF* was evaluated for each predictor based on Models 1 and 3. The maximum value of *VIF* was less than 10; hence, the effect of multi-collinearity is deemed insignificant.

Table 5. Coeffecient of variation and residual deviance for the different regression models

Model parameter	$\beta_{h/tw}$	$\beta_{bf/2tf}$	$\beta_{Lb/ry}$	$\beta_{Pc/Pyn}$	$\beta_{ln(SDR)}$	*RD*
Model 1	14.7%	**114.2%**	43.8%	7.5%	5.4%	858.42
Model 2	12.5%	-	**43.0%**	7.5%	5.4%	858.60
Model 3	10.1%	-	-	7.4%	5.4%	863.83

The process of elimination of predictor variables was finally concluded with the adoption on Model 3. Model 3 has a pseudo Cox and Snell's R^2 (Cox and Snell 1971) of 0.851 indicating that the model predicts the outcome reasonably well. This simplified, yet accurate, model utilizes only three predictors. The intercept values for each damage state *j*, α_j, and the predictors' coefficients, β, for Model 3 are summarized in Table 6 as well as their confidence band at the 90% confidence level. The regression model parameters are estimated using the maximum likelihood approach. Using the summarized parameters, the fragility function for a given damage state can be deduced. For example, the probability of reaching or exceeding DS_3 can be calculated as follows,

$$\mathrm{P}[\mathrm{DS}_3 \mid SDR_C] = 1 - \frac{e^y}{1+e^y}$$
$$\text{where, } y = \ln\left(\frac{p_3}{1-p_3}\right) = 14.664 - 0.150\cdot\left(\frac{h}{t_w}\right) - 11.081\cdot\left(\frac{P_c}{P_{yn}}\right) - 5.708\cdot\ln(SDR_C) \quad (7)$$

Table 6. Logisitic model paramters

Model parameter	α_1 [DS_1]	α_2 [DS_2]	α_3 [DS_3]	α_4 [DS_4]	$\beta_{h/tw}$	$\beta_{Pc/Pyn}$	$\beta_{ln(SDR)}$
Mean	5.515	10.753	14.664	16.695	-0.150	-11.081	-5.708
COV	12.26%	7.93%	6.61%	6.11%	10.07%	7.39%	5.38%
10%CI	4.403	9.349	13.070	15.018	-0.125	-9.734	-5.202
90%CI	6.628	12.156	16.259	18.372	-0.175	-12.429	-6.213

Figure 8 shows sample fragility surface plots for DS_3 at P_c/P_{yn} = 0.05 and 0.55. This figure demonstrates the fragility surface shifting towards lower SDR_C values (implying an increase in damage probability) when the compressive axial load increases. Furthermore, by looking at specific h/t_w or P_c/P_{yn}, the same surface plots can be transformed into the commonly used two-dimensional drift-based fragility curves. The drift-based fragility curves are deduced from the ordinal logistic regression model for selected P_c/P_{yn} and h/t_w values are shown in Fig. 9. In the same figure, the corresponding univariate lognormal fragility curve (see Fig. 5) is superimposed. For instance, at SDR_C= 2%, the univariate fragility estimates a

75% chance of local buckling initiation (see Figure 9a). However, this is strongly dependent on the applied compressive axial load ratio and the local web slenderness of the steel column of interest. The multivariate fragilities suggest that, for a column with h/t_w=40 (≈W24x103), if P_c/P_{yn} = 0.05 (low rise buildings) the corresponding P($DS_2|SDR_C$) = 40%; while if P_c/P_{yn} = 55% (as the case for columns in existing high rise buildings) then P($DS_2|SDR_C$) = 100%. Similarly, a steel column with a stockier cross-section would have a lower chance of local buckling formation at a given SDR_C (see Figure 9b). These differences become more pronounced in ultimate damage states. This is demonstrated in Figs 9c and 9d for DS_3. These figures highlight the importance of employing multivariate fragilities, whenever possible, for a more robust quantification of building-specific economic losses.

Finally, it is worth noting that if OLR is conducted with only two observation points, all the resulting fragility surfaces would marginally vary from those that are based on five observation points. In particular, in the former case, the fragility uncertainty (i.e., COV values and confidence intervals) is almost 80% higher than those of the latter case.

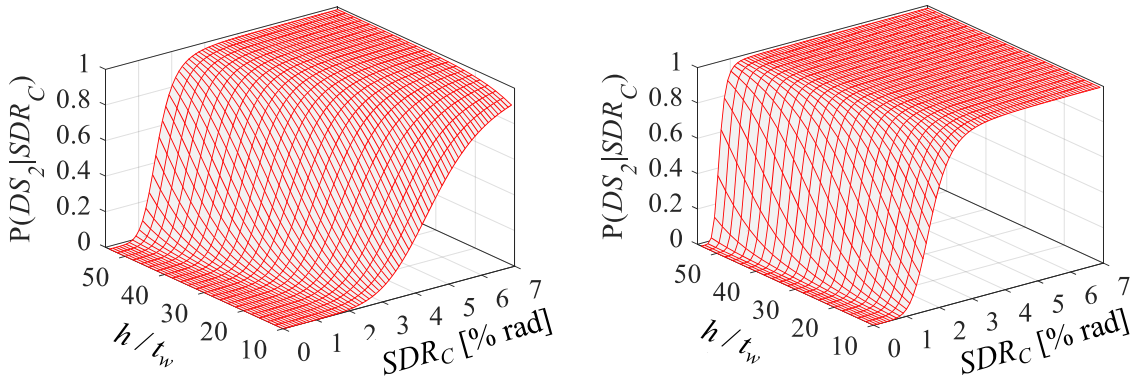

(a) P_c/P_{yn} = 0.05 (b) P_c/P_{yn} = 0.55

Figure 8. Dual-parameter fragility curves for DS_2 at different axial load ratios

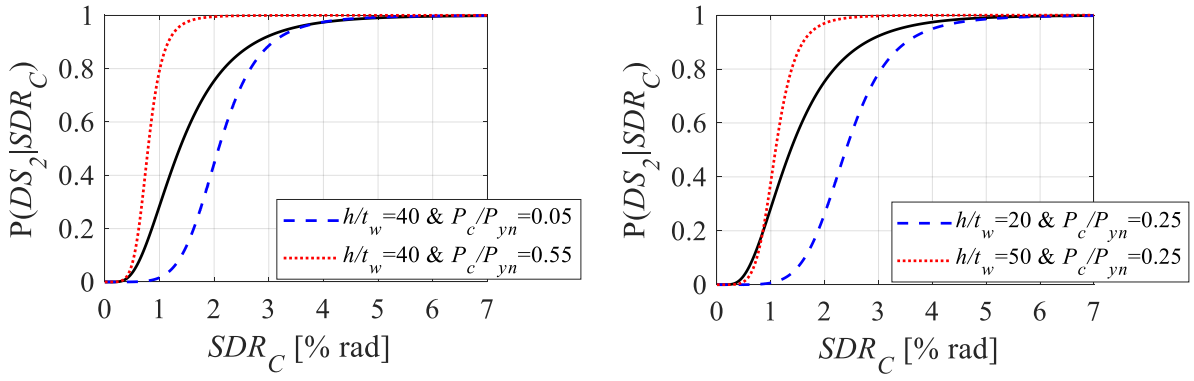

(a) DS_2: h/t_w =40 and different P_c/P_{yn} (b) DS_2: P_c/P_{yn} =0.25 and different h/t_w

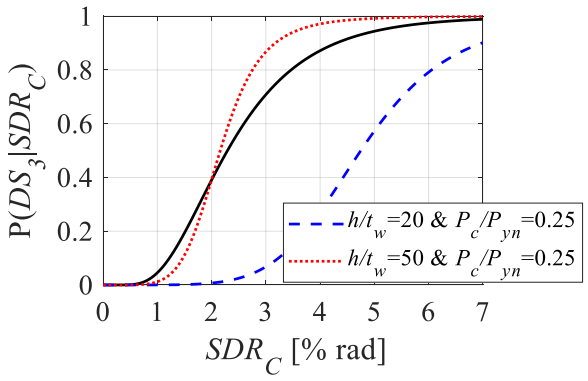

(c) DS$_3$: h/t_w =40 and different P_c/P_{yn}

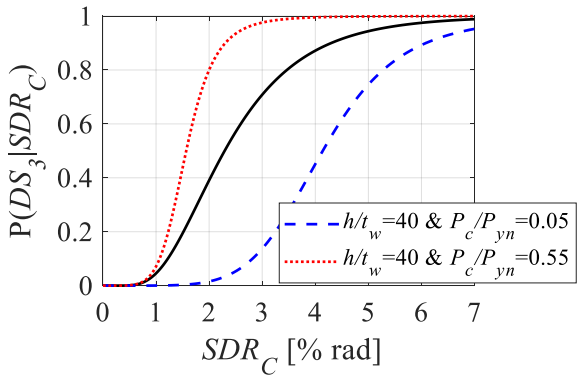

(d) DS$_3$: P_c/P_{yn} =0.25 and different h/t_w

Figure 9. Comparison between univariate (*solid line*) and multivariate (*dashed lines*) fragility curves for DS$_2$ and DS$_3$

EFFECT OF LOADING HISTORY ON COLUMN FRAGILITY CURVES

The extent of column damage is strongly dependent on the cumulative plastic deformation demands. The fragility curves discussed in previous sections were developed based on experimental data from columns subjected to typical symmetric cyclic loading histories for consistency with the component fragility database available in FEMA P58. Although this lateral loading history is representative of design-basis earthquakes (10% probability of occurrence in 50 years) where a steel MRF would typically experience inelastic drift cycles up to about 2% or less (Clark et al. 1997; Krawinkler 2009), it is not representative of low-probability of occurrence earthquakes (e.g. events with 2% probability of occurrence in 50 years). These earthquakes are characterized by a few inelastic cycles followed by asymmetric drifting in one loading direction (i.e., ratcheting) that would typically lead to residual lateral deformations. Suzuki and Lignos (2014, 2015) developed collapse-consistent histories and tested experimentally a number of wide-flange steel columns to quantify such effects and assess the differences with those subjected to standard symmetric loading histories. The same protocols were used in tests by Elkady and Lignos (2018a) and Lignos et al. (2016). Table 7 summarizes the geometric properties, axial load ratio, and the column rotations at which different damage states occur of nine specimens that were subjected to collapse-consistent lateral loading.

Table 7. Summary of experimental database for steel columns subjcted to collapse-consistant lateral loading and constant axial load

Reference	#	Section	$\frac{h}{t_w}$	$\frac{b_f}{2t_f}$	$\frac{L_b}{r_y}$	$\frac{P_c}{P_{yn}}$	SDR_C [% rad]				
							DS$_1$	DS$_2$	DS$_3$	DS$_4$	DS$_5$
Suzuki and Lignos (2015)	1	W14x53	31.6	6.3	38	0.33	0.67	1.60	8.00	12.0	12.0
	2	W14x53	32.4	6.3	38	0.33	0.76	1.20	4.00	6.00	6.40

	3	W14x61	34.3	8.1	30	0.33	0.78	2.00	6.00	7.80	10.4
	4	W14x82	22.6	6.0	29	0.33	0.65	6.20	8.00	14.0	-
Elkady and Lignos (2018a)	5	W24x146	33.3	6.1	52	0.24	0.72	1.50	6.22	-	-
	6	W24x146	32.5	6.0	52	0.22	0.72	2.50	6.20	8.90	11.6
	7	W24x84	47.0	6.1	79	0.19	0.55	1.50	5.00	10.0	10.2
	8	W24x84	47.4	6.1	80	0.19	0.58	1.50	5.00	9.00	10.0
Lignos et al. (2016)	9	W14x61	30.3	7.8	30	0.53	0.46	2.00	4.60	5.70	5.80

Although data from only nine tests are available at this point, these still permit the development of indicative univariate drift-based fragility curves to assess the differences with the ones based on symmetric loading. Table 8 summarizes the population parameter values of the fitted lognormal CDF based on a collapse-consistent loading protocol for all the damage states. Based on Figure 10, it is evident that the lateral loading history does not practically affect the onset of yielding and local buckling (DS_1 and DS_2). Notably, the ultimate damage states, DS_3 and DS_4, are significantly affected by the employed loading history. For instance, at 3% drift, a column subjected to a symmetric loading history has 80% chance of losing 20% of its flexural capacity. The same column has literally zero chance of reaching this damage state when subjected to a collapse-consistent loading history (see Figure 10c). This agrees with findings from experiments that assessed the influence of the loading history on the steel column stability (Suzuki and Lignos 2015; Lignos et al. 2016; Elkady and Lignos 2018a). These observations imply that a single set of univariate fragility curves such as those based on symmetric loading can be generically employed in loss assessment studies as long as column damage is expected to be limited to DS_1 or DS_2. Generally speaking, building specific loss-assessment shall be based on different sets of fragility curves depending on the performance level of interest (i.e., design basis or maximum considered earthquake). This is conceptually analogous with multiple stripe analysis that adapts the ground motion suites at different ground motion intensities (Lin et al. 2013). This statement is further examined in the next section where the influence of the proposed fragility curves on building specific losses is examined.

Table 8. Population parameters for univariate drift-based lognormal fragility curves for steel columns subjected to collaspe-consistent loading

Damage state	μ_{SDR_C}	$\sigma_{\ln SDR_C}$	$\mu_{SDR}\|90\%$CI (lower, upper)	$\sigma_{\ln SDR_C}\|90\%$CI (lower, upper)
DS_1 (Y)	0.646	0.173	0.627,0.666	0.124, 0.296

DS_2 (LB)	1.330	0.743	1.170,1.513	0.533, 1.271
DS_3 (MD)	5.745	0.238	5.513, 5.986	0.171, 0.407
DS_4 (SD)	7.451	0.300	7.052, 7.873	0.211, 0.538
DS_5 (ED)	9.571	0.327	9.013, 10.163	0.231, 0.587

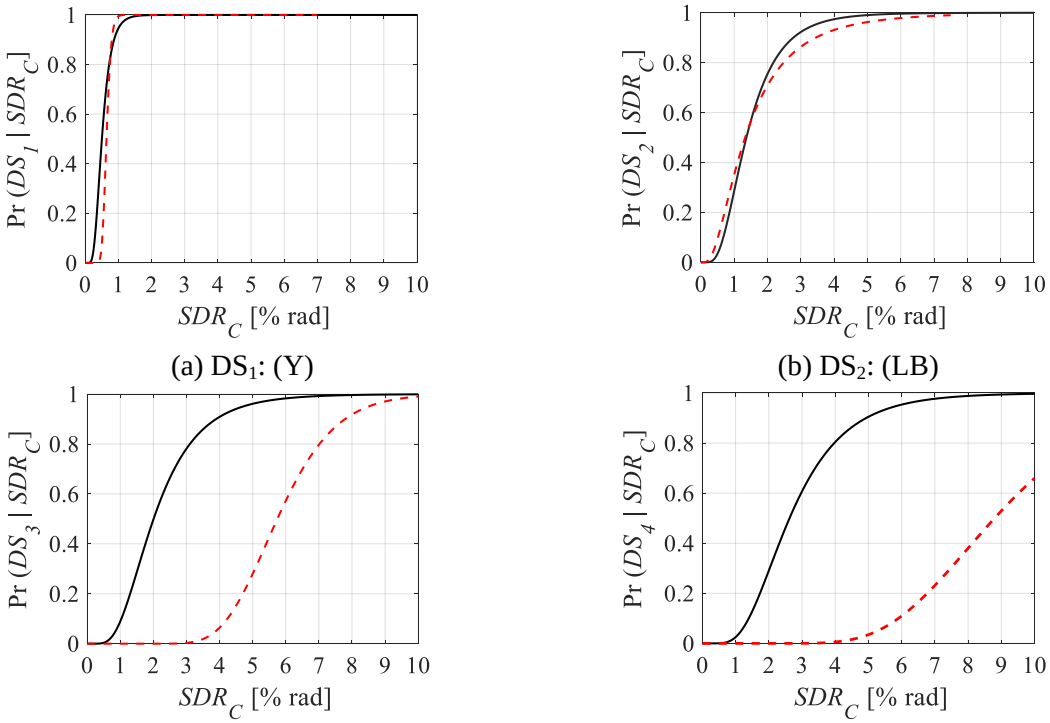

(a) DS_1: (Y) (b) DS_2: (LB)

(c) DS_3: (MD) (d) DS_4: (SD)

Figure 10. Comparison between univariate drift-based fragility curves based on symmetric (*solid line*) and collapse-consistent loading (*dashed line*)

EFFECT OF EMPLOYED FRAGILITIES ON BUILDING-SPECIFIC EARTHQUAKE-INDUCED LOSSES

This section demonstrates the implications of utilizing the proposed fragility curves for steel wide-flange columns on the expected building-specific economic losses in the aftermath of earthquakes. For this purpose, a prototype 8-story office building with perimeter special MRFs is used. This building was designed in California based on ASCE (2010). The plan and elevation views of the building as well as the main seismic design parameters and MRF member sizes are shown in Figure 11. Story-based engineering demand parameters, such as story drift ratios and floor absolute accelerations, are obtained through nonlinear-response history analyses (NRHA) using the Far-Field ground-motion set specified in FEMA P695 (FEMA 2009). Individual horizontal components of the ground-motion set were applied to the 2-dimensional numerical model of the building's EW direction. The design details and

the nonlinear model specifics of this building can be found in Elkady and Lignos (2015b). The ground-motion set is scaled to match two seismic intensities representative of design-basis and maximum-considered earthquakes (DBE and MCE, respectively). Building-specific earthquake-induced loss assessment is conducted according to Ramirez and Miranda (2012). In particular, the likelihood of building demolition due to lateral residual deformations along the building height is explicitly considered. The number of the different structural and non-structural components in this building, as well their fragility and repair cost estimates, can be found in Hwang and Lignos (2017). It should be noted that no repair cost was assigned to DS_1. The remaining column damage states where assigned repair costs similar to those specified for comparable damage states in welded beam-to-column connections (FEMA 2012). DS_2 and DS_3 are assigned repair costs of 16,033$ and 25,933$, respectively, similar to those specified for compatible damage states in welded beam-to-column connections (FEMA 2012). Similarly, DS_4 and DS_5 are assigned a repair cost of 41,869$~46,903$ (depending on the column size), which accounts for column shoring and replacement as well as replacement of the adjacent column splices.

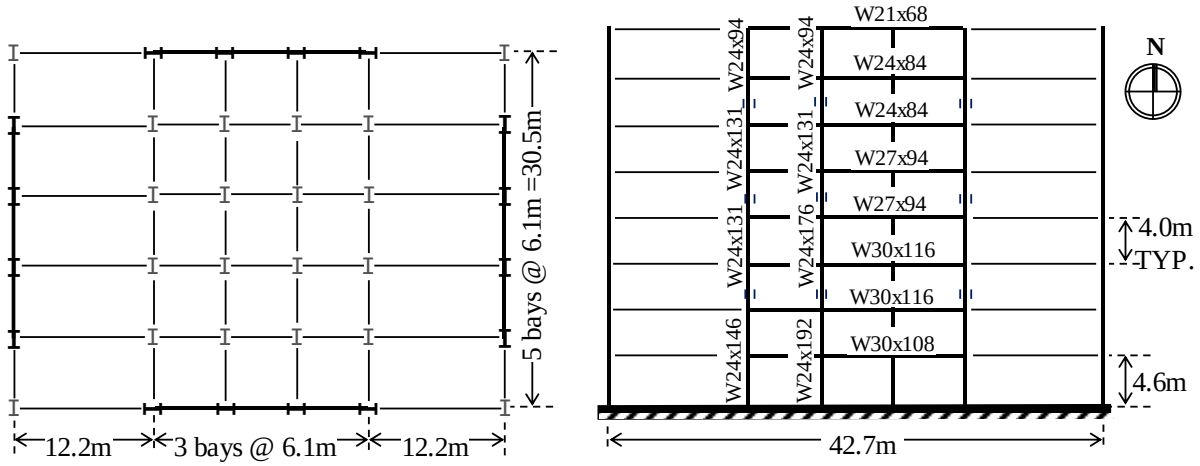

Figure 11. Plan and elevation view of the analyzed prototype 8-story building

Four cases are considered for economic loss quantification:

- Case 1: ignoring column damage, which is consistent with the assumption of FEMA P58 (FEMA 2012).
- Case 2: considering column damage by employing the univariate fragility curves based on symmetric loading (see Fig. 7).
- Case 3: considering column damage by employing the multivariate fragility curves based on OLR (see Table 6).

- Case 4: considering column damage by employing the univariate fragility curves based on collapse-consistent loading (see Fig. 10).

In cases 2 to 4, the probability of column damage (based on univariate or multivariate fragility functions) is evaluated based on the story drift-ratio demands due to column bending only if the respective column experiences plastic deformation. It is also assumed that no damage takes place in the column base connection or the underlying concrete footing. This is consistent with the current steel MRF design practice that implies such connections should remain elastic during a seismic event. In case 3, the gravity load demand was employed in the multivariate fragility curves for both interior and exterior columns For the sake of simplicity, it is assumed that damage only occurs in structural components in the EW direction assuming unidirectional ground shaking.

Figure 12 shows the disaggregation of economic losses for the two seismic intensities of interest. The results in this figure are based on the median demand parameters of the employed ground-motion set. It is evident that earthquake-induced losses are governed by non-structural component damage and demolition at DBE and MCE, respectively. Structural repair losses are further disaggregated along the height of the 8-story office building for the four analyzed cases discussed previously. The results suggest that, when the steel column damage potential is neglected (i.e., case 1), losses due to structural component repairs are underestimated by about 10% regardless of the ground motion intensity and the employed fragility curve.

Multivariate fragility curves (case 3) can capture the potential column damage variation along the building height depending on the column cross-section and the imposed axial load demand. For the 8-story building studied here, the univariate fragilities overestimated the monetary losses due to column structural damage by a factor of two compared to the multivariate ones. Similarly, at the MCE intensity, univariate fragilities based on symmetric loading (case 2) can overestimate column damage by about 50% compared to those based on collapse-consistent loading (case 4). The reduction in column damage in case 4 is driven by the fact that the first-story column base experienced a 4.3% drift, on average, (see Figures 10c-d) which corresponds to a fairly low probability of it being in or exceeding DS_3 to DS_5. The difference between case 2 and case 4 is marginal at DBE intensity because first-story columns only experienced a SDR_C =2.0%, on average. At the same intensity, upper-story columns were practically not affected by the employed fragility because the SDR_C along the building height was less than 0.8%. At MCE intensity (see Fig. 12), potential repairs due to

column damage at upper stories is also traced, although marginal in this case. This observation highlights the importance of utilizing the appropriate fragility curve family given a seismic intensity of interest and the expected column lateral drift demands. This issue deserves more attention in tall buildings engineered without capacity-design considerations (Hutt et al. 2016) or in steel MRFs subjected to near-fault ground motions where the building's fundamental period is longer than the pulse period (Alavi and Krawinkler 2004). Referring to Figure 12, a side issue is the fact that an appreciable percentage of structural repair losses is associated with damage in gravity connections. This highlights the need for enhanced gravity connections to reduce such losses (Khoo et al. 2013; Miranda et al. 2014).

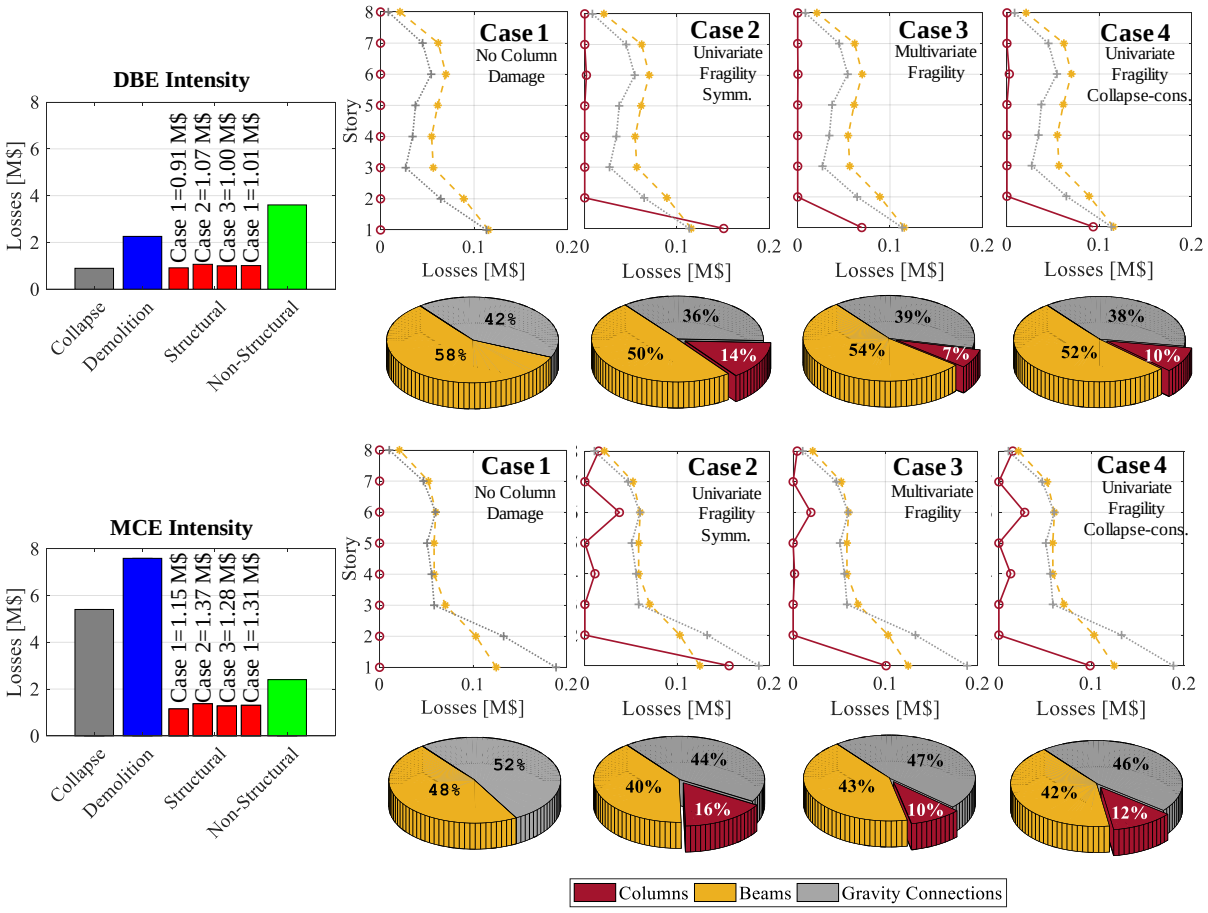

Figure 12. Influence of the employed steel column fragility curves on the disaggregated economic losses at specific seismic intensities

The expected annual losses (EALs) are deduced by integrating the earthquake vulnerability curves of the 8-story building over the site-specific seismic hazard curve from the national seismic hazard model of the United States (Petersen et al. 2008). The EALs due to structural repairs, normalized by the total building replacement cost (28M$), become more than double when the steel column damage potential is considered as shown in Fig. 13. This

is mainly attributed to damage occurring at the first-story column bases (see loss distribution along the height in Figure 12). It should be noted from the same figure that although the employed steel column fragilities affect the computed EALs, these are still dominated by repairs due to non-structural damage in acceleration-sensitive components followed by those in drift-sensitive ones. This is attributed to the fact that EALs are usually dominated by frequently occurring earthquakes rather than seismic events with a low-probability of occurrence (Hwang and Lignos 2017). It is likely that the EAL contributions may be quite different in steel frame buildings with MRFs designed in areas of moderate seismicity. This remains to be found in future studies.

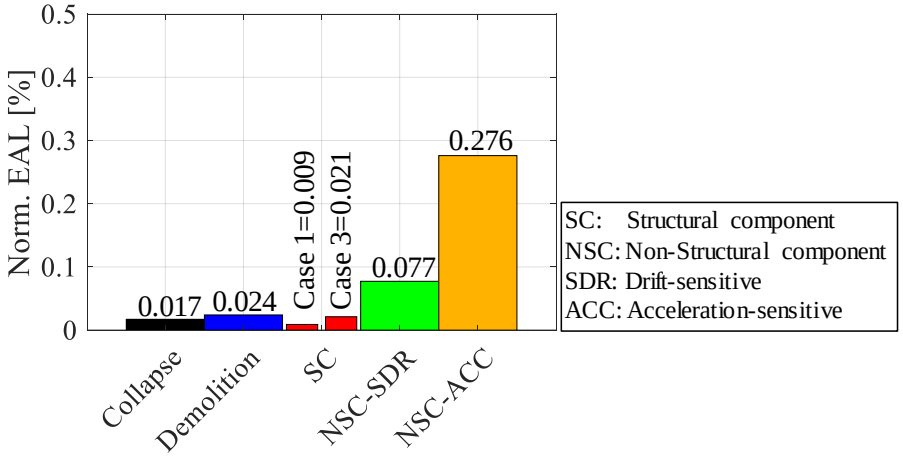

Figure 13. Influence of the employed steel column fragility curves on the expected annual losses

SUMMARY AND CONCLUSIONS

This paper proposes univariate and multivariate damage fragility curves for wide-flange steel columns in support of performance-based earthquake engineering with emphasis on building-specific loss assessment. Towards that objective, an experimental database was assembled that includes 38 compact column specimens from five different test programs conducted to date. These specimens were consistently tested under a unidirectional cyclic symmetric lateral loading protocol coupled with constant compressive axial load. Five damage states, associated with pre-defined repair measures and repair costs, were defined based on experimental observations. These include the onset of yielding and local buckling. The remaining three damage states are associated with different levels of column axial shortening and loss of flexural strength that is typically accompanied by member geometric instabilities.

Univariate drift-based lognormal fragility curves as well as their confidence bands were developed. These fragility curves are similar to those commonly used in the literature where

damage is expressed by a single predictor; the steel column story-drift demand in this case. Acknowledging the dependency of column damage on the imposed lateral loading history, another set of univariate fragilities was developed based on data from steel columns subjected to collapse-consistent lateral loading histories, representative of earthquakes with a low probability of occurrence. These fragility curves are indicative due to limited number of tests (9 in total). Under this loading history, the probability of column damage following the onset of local buckling is significantly reduced compared to symmetric loading history (representative of design-basis earthquakes) due to the lower cumulative plastic deformation demands that a steel column experiences in this case.

The steel column damage and stability are strongly dependent on its local web slenderness and axial load demand in addition to the story-drift, as observed in recent experimental studies. Acknowledging this fact, multivariate fragility curves were developed using ordinal logistic regression. While univariate fragilities are useful for the rapid loss assessment of buildings where only story-drift demands are known, multivariate fragilities can provide a more accurate structural damage estimation once the details of member sizes and axial load demands are available. Comparisons of univariate and multivariate fragility curves, for selected combinations of web slenderness and axial load demands, demonstrated the significant variability in the predicted probability of damage depending on these two parameters. This variability becomes more evident at ultimate damage states (i.e., DS_3 to DS_5).

A code-conforming 8-story building with special steel MRFs is used to demonstrate the potential implications of the developed column fragility curves on building specific loss assessment. It is found that considering column damage can increase structural repair losses by about 10% for the case study considered. The contribution of repairs due to structural damage on the expected annual losses (EALs) becomes double when the steel column damage potential is considered in the earthquake-induced loss assessment. However, the EALs are strongly influenced by repairs associated with the non-structural building content regardless of the employed steel column fragility curve. In that respect, the choice of the employed steel column fragility curve is not crucial if the objective is to estimate the EALs.

The multivariate fragility curves seem to capture the column damage variation along the building height depending on the column size and the axial load demand. For the investigated capacity-designed steel MRF building, column damage was mostly concentrated at the first-story column bottom end. However, this may not be the case in existing and/or tall buildings

or steel frame buildings designed in areas of moderate seismicity that lack capacity-design considerations.

ACKNOWLEDGMENTS

This study is based on work supported by the Swiss National Science Foundation (Award No. 200021_169248) and École Polytechnique Fédérale de Lausanne (EPFL). This financial support is gratefully acknowledged. The authors thank Dr. Seong-Hoon Hwang for his assistance with economic loss assessment. The authors sincerely thank the three anonymous reviewers of this paper for their constructing feedback and comments that significantly improved the quality of the paper. Any opinions, findings, conclusions, or recommendations expressed in this paper are those of the authors and do not necessarily reflect the views of sponsors.

REFERENCES

American Institute of Steel Construction (AISC), 2016a. *Seismic provisions for structural steel buildings, ANSI/AISC 341-16*, Chicago, IL.

American Institute of Steel Construction (AISC), 2016b. *Specification for structural steel buildings, ANSI/AISC 360-16*, Chicago, IL.

Alavi, B., and Krawinkler, H., 2004. Behavior of moment-resisting frame structures subjected to near-fault ground motions. *Earthquake Engineering & Structural Dynamics*, **33**(6), 687-706.

American Society of Civil Engineers (ASCE), 2010. *Minimum design loads for buildings and other structures, ASCE/SEI 7-10*, Reston, VA.

Aslani, H., and Miranda, E., 2005. *Probabilistic earthquake loss estimation and loss disaggregation in buildings, Report No. 157*Stanford, CA.

Chatterjee, S., and Hadi, A. S. (2015). *Regression analysis by example*, Fifth Edition, John Wiley & Sons.

Chiozzi, A., and Miranda, E., 2017. Fragility functions for masonry infill walls with in-plane loading. *Earthquake Engineering & Structural Dynamics*, **46**(15), pp 2831–2850.

Clark, P., Frank, K., Krawinkler, H., and Shaw, R., 1997. *Protocol for fabrication, inspection, testing, and documentation of beam-column connection tests and other experimental specimens*, *Report No. SAC/BD-97/02*, SAC Joint Venture, Sacramento, CA, USA.

Cornell, C. A., and Krawinkler, H., 2000. Progress and challenges in seismic performance assessment. *PEER Center News*, **3**(2), 1-3.

Cox, D. R., and Snell, E. J. 1971. On test statistics calculated from residuals. *Biometrika*, **58**(3), 589-594.

Crow, E. L., Davis, F. A., and Maxfield, M. W. (1960). *Statistics manual*, Dover Publication INC., New York, USA.

Elkady, A., and Lignos, D. G., 2015a. Analytical investigation of the cyclic behavior and plastic hinge formation in deep wide-flange steel beam-columns. *Bull Earthquake Eng*, **13**(4), 1097-1118.

Elkady, A., and Lignos, D. G., 2015b. Effect of gravity framing on the overstrength and collapse capacity of steel frame buildings with perimeter special moment frames. *Earthquake Engineering & Structural Dynamic*, **44**(8), 1289–1307.

Elkady, A., and Lignos, D. G., 2016. Dynamic stability of deep and slender wide-flange steel columns – full scale experiments, *in Proceedings, ASCE Annual Stability Conference*, April 12-15, 2016, Orlando, Florida, USA.

Elkady, A., and Lignos, D. G., 2017. Stability requirements of deep steel wide-flange columns under cyclic loading, *in Proceedings, ASCE Annual Stability Conference*, March 21-24, 2017, San Antonio, Texas, USA.

Elkady, A., Cravero, J., and Lignos, D. G., 2018. Steel columns under multi-axis seismic loading: Experimental findings and design recommendations. *in Proceedings, Behaviour of Steel Structures in Seismic Areas*, Febrauary 14-17, 2018, Christchurch, New Zealand.

Elkady, A., and Lignos, D. G., 2018a. Full-scale testing of deep wide-flange steel columns under multi-axis cyclic loading: Loading sequence, boundary effects and out-of-plane brace force demands. *ASCE Journal of Structural Engineering*, **144**(2).

Elkady, A., and Lignos, D. G., 2018b. Improved seismic design and nonlinear modeling recommendations for wide-flange steel columns. *ASCE Journal of Structural Engineering*,

Federal Emergency Management Agency (FEMA), 2009. *Quantification of building seismic performance factors*, *Report FEMA-P695*, Washington, DC.

Federal Emergency Management Agency (FEMA), 2012. *Seismic performance assessment of buildings*, *Report FEMA P-58-1*, Washington, DC.

Gardoni, P., Der Kiureghian, A., and Mosalam, K. M., 2002. Probabilistic capacity models and fragility estimates for reinforced concrete columns based on experimental observations. *Journal of Engineering Mechanics*, **128**(10), 1024-1038.

Gulec, C. K., Gibbons, B., Chen, A., and Whittaker, A. S., 2011. Damage states and fragility functions for link beams in eccentrically braced frames. *Journal of Constructional Steel Research*, **67**(9), 1299-1309.

Gupta, A., and Krawinkler, H., 2000. Behavior of ductile SMRFs at various seismic hazard levels. *Journal of Structural Engineering*, **126**(1), 98-107.

Hartloper, A., and Lignos, D. G. 2017. Updates to the ASCE-41-13 provisions for the nonlinear modeling of steel wide-flange columns for performance-based earthquake engineering, *in*

Proceedings, 8th European Conference on Steel and Composite Structures, September 13-15, 2017, Copenhagen, Denmark.

Hutt, C. M., Almufti, I., Willford, M., and Deierlein, G., 2016. Seismic loss and downtime assessment of existing tall steel-framed buildings and strategies for increased resilience. *Journal of Structural Engineering*, **142**(8).

Hwang, S. H., and Lignos, D. G., 2017. Earthquake-induced loss assessment of steel frame buildings with special moment frames designed in highly seismic regions. *Earthquake Engineering & Structural Dynamics*, **46**(13), 2141-2162.

Khoo, H.-H., Clifton, C., Butterworth, J., and MacRae, G., 2013. Experimental study of full-scale self-centering sliding hinge joint connections with friction ring springs. *Journal of Earthquake Engineering*, **17**(7), 972-997.

Kolmogorov, A., 1933. Sulla determinazione empirica di una legge di distributione. *Giornale dell' Instituto Italiano delgi Attuari (in italian)*, **4**, 1-11.

Krawinkler, H., 1996. Cyclic loading histories for seismic experimentation on structural components. *Earthquake Spectra*, **12**(1), 1-12.

Krawinkler, H., 2009. Loading histories for cyclic tests in support of performance assessment of structural components, *in Proceedings, 3rd International Conference on Advances in Experimental Structural Engineering*, October 15-16, 2009, San Francisco, CA, USA.

Kutner, M. H., Nachtsheim, C., and Neter, J. (2004). *Applied linear regression models*, 4th Edition, McGraw-Hill/Irwin.

Lee, K., and Foutch, D. A., 2002. Seismic performance evaluation of pre-northridge steel frame buildings with brittle connections. *Journal of Structural Engineering*, **128**(4), 546-555.

Lignos, D. G., Cravero, J., and Elkady, A., 2016. Experimental investigation of the hysteretic behavior of wide-flange steel columns under high axial load and lateral drift demands, *in Proceedings, 11th Pacific Structural Steel Conference*, October 26-28, 2016, Shanghai, China.

Lignos, D. G., and Karamanci, E., 2013. Drift-based and dual-parameter fragility curves for concentrically braced frames in seismic regions. *Journal of Constructional Steel Research*, **90**, 209-220.

Lignos, D. G., Kolios, D., and Miranda, E., 2010. Fragility assessment of reduced beam section moment connections. *Journal of Structural Engineering*, **136**(9), 1140-1150.

Lin, T., Haselton, C. B., and Baker, J. W., 2013. Conditional spectrum-based ground motion selection. Part i: Hazard consistency for risk-based assessments. *Earthquake Engineering & Structural Dynamics*, **42**(12), 1847-1865.

MacRae, G. A., Carr, A. J., and Walpole, W. R., 1990. *The seismic response of steel frames*, *Report No. 90-6*, Department of Civil Engineering, University of Canterbury, New Zealand.

McCullagh, P., 1980. Regression models for ordinal data. *Journal of the Royal Statistical Society, Series B*, **42**(2), 109-142.

Miranda, E., Medina, R., Mosqueda, G., Lignos, D. G., Fell, B., Eads, L., Hashemi, J., Zargar, S., and Negrete, M., 2014. Collapse assessment of multi-story buildings through hybrid testing, *in Proceedings, 10th National Conference on Earthquake Engineering*, July 21-25, 2014, Anchorage, AK, USA.

Newell, J. D., and Uang, C.-M., 2006. *Cyclic behavior of steel columns with combined high axial load and drift demand, Report No. SSRP-06/22*, Department of Structural Engineering, University of California, San Diego.

Ozkula, G., Harris, J., and Uang, C. M., 2017. Observations from cyclic tests on deep, wide-flange beam-columns. *AISC Engineering Journal*, **54**(1), 45-61.

Petersen, M. D., Frankel, A. D., Harmsen, S. C., Mueller, C. S., Haller, K. M., Wheeler, R. L., Wesson, R. L., Zeng, Y., Boyd, O. S., and Perkins, D. M., 2008. *Documentation for the 2008 update of the united states national seismic hazard maps*, Geological Survey (US).

Popov, E. P., Bertero, V. V., and Chandramouli, S., 1975. *Hysteretic behavior of steel columns, Report No. EERC 75-11*, Earthquake Engineering Research Center, Berkeley, CA, USA.

Ramirez, C. M., Lignos, D. G., Miranda, E., and Kolios, D., 2012. Fragility functions for pre-northridge welded steel moment-resisting beam-to-column connections. *Engineering Structures*, **45**(Supplement C), 574-584.

Ramirez, C. M., and Miranda, E., 2012. Significance of residual drifts in building earthquake loss estimation. *Earthquake Engineering & Structural Dynamics*, **41**(11), 1477-1493.

Reed, D. A., Friedland, C. J., Wang, S., and Massarra, C. C., 2016. Multi-hazard system-level logit fragility functions. *Engineering Structures*, **122**, 14-23.

Retamales, R., Davies, R., Mosqueda, G., and Filiatrault, A., 2013. Experimental seismic fragility of cold-formed steel framed gypsum partition walls. *Journal of Structural Engineering*, **139**(8), 1285-1293.

Roeder, C. W., Lumpkin, E. J., and Lehman, D. E., 2012. Seismic performance assessment of concentrically braced steel frames. *Earthquake Spectra*, **28**(2), 709-727.

Ruiz-García, J., and Negrete, M., 2009. Drift-based fragility assessment of confined masonry walls in seismic zones. *Engineering Structures*, **31**(1), 170-181.

Smirnov, H., 1939. Sur les ecarts de la courbe de distribution empirique. *Recueil Mathematique (in french)*, **6**, 3-26.

Statistical Package for the Social Sciences (SPSS), 2017. *IBM Corp. Released 03-2017*, Armonk, NY, USA.

Suzuki, Y., and Lignos, D. G., 2014. Development of loading protocols for experimental testing of steel columns subjected to combined high axial load and lateral drift demands near collapse, *in*

Proceedings, 10th National Conference on Earthquake Engineering, July 21-25, 2014, Anchorage, Alaska, USA.

Suzuki, Y., and Lignos, D. G., 2015. Large scale collapse experiments of wide-flange steel beam-columns, *in Proceedings, 8th International Conference on Behavior of Steel Structures in Seismic Areas*, July 1-3, 2015, Shanghai, China.

Taghavi, S., and Miranda, E., 2003. *Response assessment of nonstructural building elements*, *PEER Report 2003/05*, Pacific Earthquake Engineering Research Center (PEER), Berkeley, CA.

Uniform Building Code(UBC), 1973. *International Conference of Building Officials*, Whittier, CA

Yazdi, A. J., Haukaas, T., Yang, T., and Gardoni, P., 2016. Multivariate fragility models for earthquake engineering. *Earthquake Spectra*, **32**(1), 441-461.